INVITED PAPER Special Section on EU's FP7 ICT R&D Project Activities on Future Broadband Access Technologies

Power Line Communications: understanding the channel for physical layer evolution based on filter bank modulation

Andrea M. TONELLO[†a)], ***Member***, **Alberto PITTOLO**[†b)], ***and*** **Mauro GIROTTO**[†c)], ***Nonmembers***

SUMMARY This paper provides an overview of power line communication (PLC) applications, challenges and possible evolution. Emphasis is put on two relevant aspects: a) channel characterization and modeling, b) filter bank modulation for spectral efficient transmission. The main characteristics of both the indoor channel (in-home, in-ship, in-car) and the outdoor low voltage and medium voltage channels are reported and compared. A simple approach to statistically model the channel frequency response (CFR) is described and it is based on the generation of a vector of correlated random variables. To overcome the channel distortions, it is shown that filter bank modulation can provide robust performance. In particular, it is shown that the sub-channel spectral containment of filtered multitone modulation (FMT) can provide high notching capability and spectral efficiency. Reduced complexity can be obtained with a cyclic filter bank modulation approach that we refer to as cyclic block FMT modulation (CB-FMT) which still provides higher spectral flexibility/efficiency than OFDM.

key words: *power line communications, power line channel, channel model, filter bank modulation.*

1. Introduction

The desire to deliver new communication services without requiring significant investments in the expansion of the telecommunication infrastructure has pushed the development of no-new-wire technologies. Besides wireless and twisted pair copper systems, PLC enables the delivery of a broad range of services exploiting power delivery grids. Since power lines are pervasively deployed, the use of PLC is potentially ubiquitous.

1.1 Some History about PLC, Applications and Standards

PLC is not a recent idea: it was used by power utilities since about 1920, initially for communications over high voltage lines between remote stations. Since then, the application areas have significantly expanded [1]. Broad band internet access offered by PLC, over the distribution network that feeds houses and buildings, was considered of great interest especially in the first decade of the new millennium. Advanced technology was deployed and it proved to be a technically valuable solution. However, the market was already highly penetrated by DSL technology which relegated PLC in few areas, although still some hope exists about its wide use in emerging countries.

In parallel, it was recognized that high speed data coming from last mile communication systems, e.g., DSL and optical fiber, might have found a bottleneck at the house door. Therefore, high speed in-home connectivity was also desirable allowing the home gateway to provide uninterrupted flow of heterogeneous traffic between the outdoor and the indoor network, the service provider and the end user. Wi-Fi has fostered such a paradigm and it has been largely researched, developed and marketed (see the evolution of the IEEE 802.11 standard). However, wireless technology may also experience complications mostly due to unfavorable propagation conditions and limited radiated power for safety reasons that do not allow to grant full coverage at the promised speeds, e.g., in multiple floor dwellings with the presence of reinforced concrete floors. Consequently, complementary technologies were also researched, and PLC found a fertile market where to prove its own validity. Initially, a number of proprietary solutions were developed, but the key for wide deployment was standardization.

A first relevant industry standard was promoted by the HomePlug (HP) Alliance that developed a broadband solution operating in the 2-28 MHz band based on orthogonal frequency division multiplexing (OFDM). The first version HP 1.0 was capable to deliver up to 14 Mbps, the second version HPAV reached a peak rate of 200 Mbps, and the latest version HPAV2 [2], completed in 2012, promises 2 Gbps of peak rate thanks to the extended bandwidth up to 86 MHz, multiple wire transmission (MIMO), precoding and adaptation together with a number of advanced techniques at the MAC layer. However, the first world wide broad band (BB) standard was IEEE P1901 which was ratified in 2010 [3], followed by ITU G.9960 (known as G.hn) [4].

More recently, the high momentum gained by the smart grid concept has reinvigorated research in PLC and in particular of so called narrow band PLC (NB PLC) technology operating in the CENELEC bands (3–148.5 kHz), in the ARIB bands (10–450 kHz) and in the FCC bands (9–490 kHz). Although the first solutions deployed single carrier modulation (e.g. frequency shift keying (FSK) in the IEC 61334 [5] standard), OFDM was chosen to provide higher speeds in the PRIME and G3 specifications [6], [7]. PRIME and G3 were the basis for the definition of the ITU G.9902 (known as G.hnem) [8]) and the IEEE P1901.2 [9] standards for the use of frequency bands below 500 kHz (ratified at the end of 2012 and 2013, respectively) and data rates up to 500 kbps.

PLC can be applied to provide two-way communication in all three smart grid domains, namely transmission,

Manuscript received January 10, 2014.
[†]The authors are with the University of Udine, Italy.
a) E-mail: tonello@uniud.it
b) E-mail: alberto.pittolo@uniud.it
c) E-mail: mauro.girotto@uniud.it
DOI: 10.1587/transcom.E0.B.1

distribution and user domains, exploiting high voltage (HV), medium voltage (MV) and low voltage (LV) lines [10]. It can be used to deliver several applications, for instance, remote fault detection, remote station surveillance, or state estimation. It can provide communication capabilities between sensors located in substations so that status can be monitored, and faults detected and isolated. PLC can also be exploited for the detection of islanding events. The main application in the LV part of the network is automatic/smart metering. For this application, PLC has already enjoyed a great deployment success, with about 90 million meters installed in Europe, and many more installed worldwide. Sensing, command, and control applications are also of great interest for applications inside home or building. The in-home PLC network can be exploited for energy management purposes, together with a wide set of home automation applications for increasing security, comfort and life quality. Two further PLC application areas lie in the management and control of micro grids, e.g. local generation grids using renewable energy sources such as solar cells and wind turbines, and in the connection between electrical vehicles and the grid, which can offer a wide set of applications.

There are a number of other application of PLC among which a promising one, but not yet significantly exploited, is in-vehicle (car, ship, plane, train) communication.

1.2 Open Challenges and Paper Contribution

Despite the existence of commercial PLC systems and recently released standards, PLC can still evolve and advanced solutions can be identified to better solve the open challenges which mostly rely on the full understanding of the hostile communication medium, the development of ad hoc modulation and coding techniques, the definition of MAC protocols for lossy channels with time variant behavior in terms of traffic, noise sources and topology changes.

In this paper, challenges and efforts in channel characterization and modeling are reported in Section 2 and Section 3, respectively. A simple vector channel model is presented in Section 3. Physical layer performance is inferred in Section 4. The principles and the rationale for the use of advanced multicarrier modulation schemes are outlined in Section 5. Finally, the conclusions follow in Section 6.

2. Channel Characterization

The characterization of the PLC channel is very important since it allows the development of models and the design of appropriate physical layer transmission technology. The specific characteristics depend on the application scenario and on the used transmission bandwidth. In general, the channel exhibits multipath propagation due to line discontinuities and unmatched loads, which translates in severe frequency selectivity. Differently from wireless, there is no mobility so that the channel is mostly static. However, changes in the wiring topology and the connected loads induce a change in the channel response. Furthermore, cyclic time variations with periodicity equal or double the mains frequency can be present [11]. This is due to the periodic change of the loads impedance with the mains frequency, in particular of those that have rectifying units and AC/DC converters that exhibit a bistatic impedance behavior. Such cyclic time variations are mostly visible at frequencies below 2 MHz. This is because most of the active loads deploy EMI filters that at high frequencies provide a (low) and stable value of impedance [12].

In order to statistically characterize the channel, we consider three physical quantities: the average channel gain (ACG), the root-mean-square delay spread (RMS-DS) and the coherence bandwidth (CB). Let us denote with $h(t)$ the channel impulse response assumed to have duration D, and with $H(f)$ the channel frequency response (CFR) assumed in the band $[F_1, F_2]$. Then, the ACG provides the average attenuation (averaged along frequencies) of the channel and it is defined as

$$G = \frac{1}{F_2 - F_1} \int_{F_1}^{F_2} |H(f)|^2 df. \tag{1}$$

The RMS-DS accounts for the energy dispersion of the channel impulse response and it is defined as

$$\sigma_\tau = \sqrt{\int_0^D \tau^2 \mathcal{P}(\tau) d\tau - \left(\int_0^D \tau \mathcal{P}(\tau) d\tau\right)^2} \quad [\mathrm{s}], \tag{2}$$

where the power delay profile, namely $\mathcal{P}(\cdot)$, is given by $\mathcal{P}(t) = |h(t)|^2 / \int_0^D |h(\tau)|^2 d\tau$. The CB at level ρ, B_c^ρ, is the frequency for which the absolute value of the correlation function $R(\nu)$ falls below ρ times its maximum, i.e., $B_c^\rho = B \quad \text{s.t.} \quad |R(B)| = \rho |R(0)|$ with

$$R(\nu) = \int_{F_1}^{F_2} H(f + \nu) H^*(f) df. \tag{3}$$

In this paper the focus is on BB channels, thus in the frequency range above 1.8 MHz, as specified by the HPAV2 standard [2]. Three different scenarios are analyzed: LV in-home, LV in-ship and in-car. We also discuss the outdoor LV and MV characteristics.

2.1 Indoor Channel

In-home LV grids are characterized by a layered tree structure with wires that depart from the main panel, reach derivation boxes and then the final outlets [13]. The presence of many branches give rise to severe frequency selective fading. In the following, we report the results of the analysis of 1300 channel responses acquired in Italian home networks. The considered bandwidth is 1.8–100 MHz. In Fig. 1a, we report the scatter plot of the RMS-DS as a function of the ACG (in dB scale). The robust fit is also reported. The two quantities are negatively related. In [14] and [15], a similar study was performed for two sets of experimental data. The former is the result of a measurement campaign in

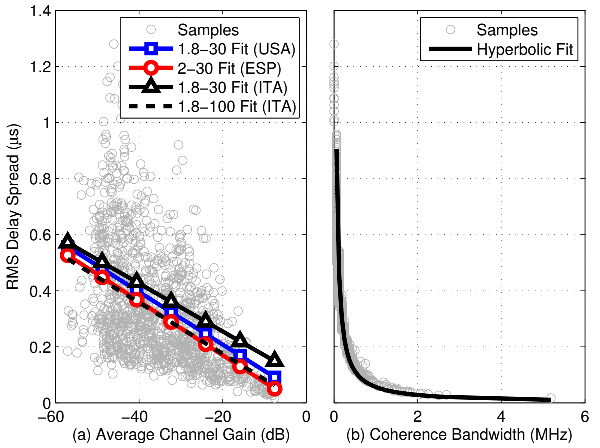

Fig. 1 RMS-DS versus ACG (a) and CB (b) for in-home channels. The robust regression fit (on left) and the hyperbolic fit (on right) are displayed.

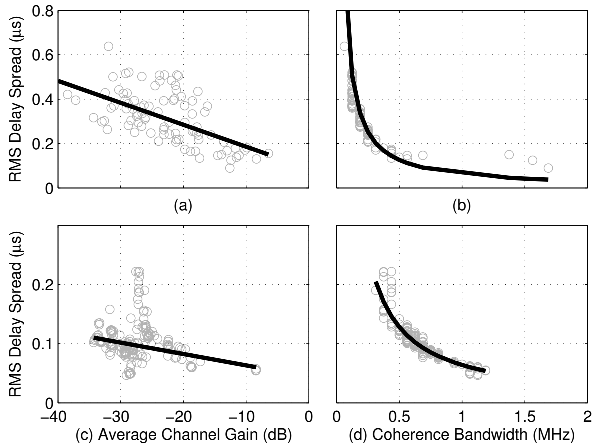

Fig. 2 RMS-DS versus ACG (on left) and CB (on right) for in-ship (on top) and in-car (on bottom) channels. The robust regression fit, in (a), (c) and the hyperbolic fit, in (b), (d), are also shown.

the United States (USA) for the 1.8–30 MHz band. The latter reports results obtained in Spain (ESP) for the 2–30 MHz band. In order to compare the results, in Fig. 1a, the robust regression fit of our data in the 1.8–30 MHz frequency range is also shown. A good agreement, especially with the ESP case, can be observed. Slight deviations of the lines slope and y-intercept may be due to the different frequency range, and differences on the procedure adopted to compute the channel impulse response that are reflected on the value of the delay spread.

Fig. 1b shows the relation between the coherence bandwidth $B_c^{0.9}$ and the delay spread of the measured channels. The samples are distributed according to a hyperbolic trend, also depicted in Fig. 1b, that reads $B_c^{0.9} = 0.057/\sigma_\tau$. A very similar relation was found in [16], for a set of channels measured in France which is $B_c^{0.9}\sigma_\tau = 0.055$.

2.2 In-Ship and In-Car Channels

In this section, we compare the in-ship scenario with the in-car environment. In the former case, we consider the data acquired in a measurement campaign made over the LV distribution network of a large cruise ship [17]. The considered channels are correspondent to two distribution grid sections: the one with a star topology from the substation switchboard to the distribution boards, and the one with a bus bar structure from the distribution board to the room panels. For the in-car case, we consider the measurement database made available and described in [18].

We focus on the mutual dependence of the statistical metrics (ACG, RMS-DS and CB), that are defined in Section 2. In particular, Fig. 2 shows the scatter plot of the RMS-DS versus the ACG and the CB, as well as the hyperbolic and the robust regression fit, for both the in-ship and the in-car scenarios. As can be noted, the robust fit slope for the in-ship scenario (Fig. 2a) is roughly five times the slope of the in-car scenario (Fig. 2c). Moreover, the in-car scenario experiences lower delay spread but similar attenuation, as clarified in Table 1. With respect to the CB, instead, the in-ship case (Fig. 2b) and the in-car case (Fig. 2d) have approximately the same hyperbolic trend (see Table 2 for details). To aid the comparison, the values of slope and y-intercept, of the robust regression fit, and the coefficient of the hyperbolic fit, for the different considered scenarios are reported in Table 2. Differences w.r.t. the results reported in [17], [19] are amenable to the way the CIR has been computed. It should be noted that the robust regression fit slope of the in-ship scenario is close to that of the in-home case in the 1.8–100 MHz frequency band.

2.3 Outdoor LV and MV Channels

Differently from the indoor scenario, a less comprehensive analysis of the outdoor PLC channel is available in the literature for what concerns both the LV and MV part of the distribution grid. A measurement campaign of the LV outdoor channel was performed by the open PLC European research

Table 1 Average statistical metrics for different channel scenarios in different frequency bands.

Scenario	Band (MHz)	$\overline{ACG}$ (dB)	$\overline{DS}$ (μs)	$\overline{CB}$ (kHz)
In-Home	1.8–100	−35.41	0.337	288.11
In-Home	1.8–50	−33.10	0.357	251.48
In-Ship	1.8–50	−22.89	0.320	258.83
In-Car	1.8–50	−27.33	0.102	677.14
Outdoor LV	1.8–50	−56.96	0.581	140.63
Outdoor MV	1.8–50	−44.39	0.722	399.59

Table 2 Robust fit parameters for RMS-DS versus ACG and hyperbolic fit coefficient for RMS-DS versus CB in different scenarios.

Scenario	Band (dB)	Robust fit		Hyperbolic fit
		slope ($\times 10^{-3}$)	y-intercept	
In-Home	1.8–100	−9.129	−0.007	0.057
In-Home	1.8–50	−8.794	0.040	0.055
In-Ship	1.8–50	−9.883	0.087	0.063
In-Car	1.8–50	−1.926	0.044	0.064

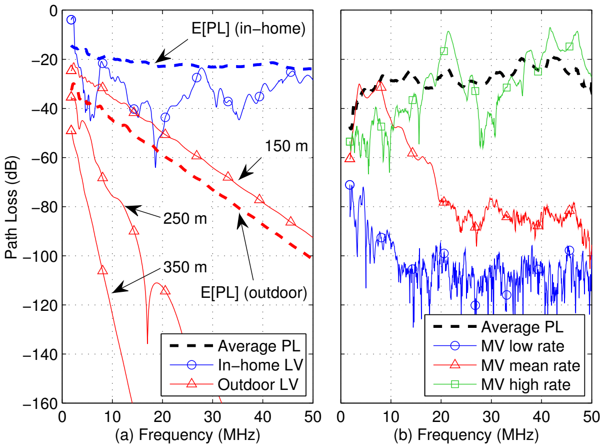

Fig. 3 Path loss for outdoor (OPERA) and in-home low voltage (a), and medium voltage (b) channels.

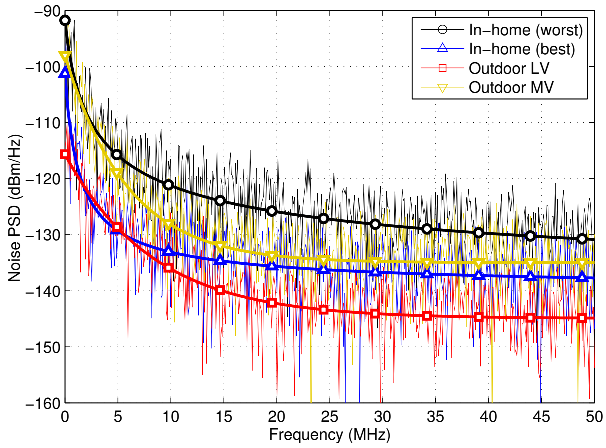

Fig. 4 Power spectral density for indoor (worst and best case) and outdoor (LV and MV) background noise. The noise model is also shown.

alliance (OPERA) project [20]. From the measurements, a deterministic model was proposed so that 8 reference channel responses have been tabulated.

Fig. 3a shows the frequency response of three different OPERA reference channels, corresponding to high (350 m), medium (250 m) and low (150 m) attenuation and decreasing path length. The average path loss profile $\overline{PL} = 10\log_{10} E[|H(f)|^2]$, where $E[\cdot]$ denotes the expectation, obtained from the full set of 8 responses is also reported. For comparison a typical in-home channel response is also shown. As can be noted, the in-home channel exhibits high frequency selectivity but lower attenuation, due to a very high number of branches, discontinuities and unmatched loads, as well as the deployment of short cables. Contrariwise, the outdoor LV channels introduce high attenuation but negligible fading effects. Cable attenuation dominates w.r.t. multipath fading.

We now consider the MV channel analyzing data obtained in a measurement campaign performed in northern Italy in 2013 and consisting of 122 responses. In Fig. 3b, the path loss for a good, a medium and a bad outdoor MV channel realization (ranked according to the capacity/rate they offer), as well as the average path loss, are depicted. It should be noted that such channels are less attenuated than the LV outdoor channels. Furthermore, the average path loss profile is only slightly worse than the indoor LV case. Some further analysis of the outdoor MV channel in a grid feeding an industrial scenario is presented in [21].

2.4 Remarks

In order to compare the different scenarios, Table 1 reports the average ACG, RMS-DS and CB values. For the in-home scenario, besides the 1.8–100 MHz frequency range, also the 1.8–50 MHz is considered for a fair comparison with the other scenarios, where acquisitions are limited at 50 MHz.

The highest ACG is experienced by the in-ship channels. This is probably due to the fact that many channels belong to a section of the grid having a star style configuration with a reduced number of branches and discontinuities. The in-car environment has the second highest ACG which is due to the shortness of the communication links. For the same reason this scenario presents the lowest RMS-DS, followed by the in-ship and the in-home case, respectively. The outdoor LV and MV channels have lower values of ACG and higher RMS-DS, due to the length of paths. The coherence bandwidth is approximately the inverse of the delay spread, thus a low delay spread implies a high coherence bandwidth and viceversa, as shown in Table 1.

As can be seen in Fig. 3, both the LV and MV outdoor channels have a decreasing path loss profile with frequency. This fact, together with the need of delivering low data rate services has pushed the development of PLC technology operating at low frequencies. However, it should be observed that what concurs to achieve good performance is not simply the good channel response but also the low presence of noise. In fact, channel capacity (and thus achievable rate by practical transmission schemes) is determined by the signal-to-noise ratio (SNR) at the receiver. The noise in PLC is a combination of several contributions: the background stationary noise, the impulsive noise with both periodic and aperiodic components which is introduced by noisy loads, switching devices and plug-in/plug-out procedures [1]. Often, the overall noise contribution is estimated by measuring the power spectral density (PSD) of the noise averaged over a long period of time. Typical noise PSD profiles are reported in Fig. 4 for the indoor and outdoor scenarios. The figure shows an exponentially decreasing profile which can be modeled for the in-home scenario as [22]

$$PSD_W^{IH}(f) = a + b|f|^c \quad [\text{dBm/Hz}], \tag{4}$$

while for the outdoor LV and MV scenarios as [23]

$$PSD_W^{LV,MV}(f) = a + be^{fc} \quad [\text{dBm/Hz}]. \tag{5}$$

for a certain choice of the parameters a, b, c, which may be different for each model and scenario. Interestingly, even the best indoor case (lowest noise possible) exhibits a noisier environment compared to the outdoor LV case. The average SNR at the receiver, taking into account the effect of the channel can be computed according to the equation

$$\overline{SNR} = E\left[\frac{\int_{F_1}^{F_2} P_S(f)|H(f)|^2 df}{\int_{F_1}^{F_2} P_W(f) df}\right] \quad \text{[dB]}. \tag{6}$$

where $P_S(f)$ and $P_W(f)$ denote the transmitted signal and the noise PSD. For instance, in the outdoor LV scenario, assuming a transmission at a constant PSD level of −50 dBm/Hz, the average SNR for the CENELEC 3–148.5 kHz band, the FCC 9–490 kHz and the 1.8–30 MHz BB, is equal to 34.86, 37.34 and 39.65 dB, respectively. This shows that potentially higher SNRs are experienced with the use of BB PLC than with NB PLC in the smart grid context. In turn, BB PLC has the potentiality to offer higher noise margins and not only higher achievable rates. This has also been shown with a comparison between the use of NB OFDM and impulsive ultra wide band (UWB) modulation in [24]. However, BB PLC may undergo more severe limitations to grant EMC and coexistence according to current norms.

3. PLC Channel Modeling

Despite the fact that the PLC channel appears to have an unpredictable behavior, significant progress has been made in terms of modeling. There are typically two approaches that are referred to as top-down and bottom-up. Initially, deterministic models were developed and more recently statistical models have been proposed.

In the top-down approach, the channel response is obtained by fitting a certain parametric analytic function with data coming from the experimental measures. In particular, the multipath nature of the channel, as well as the effect of lossy cables, were captured by the frequency response deterministic model in [25]. The idea of developing a statistical top-down model by introducing some variability in the model in [25] was firstly presented in [26]. The refinement of such a model to fit experimental data from an in-home measurement campaign up to 100 MHz was done in [27]. Another statistical model of the CFR was proposed in [28], while a simple time-domain multipath random generator was presented in [14].

The bottom-up approach, instead, models the channel transfer function exploiting the transmission line theory. Therefore, its application requires the knowledge of the network topology in terms of wiring cables and loads. The complex structure of the network can be described via ABCD or scattering parameter matrices [29]. A first proposal to use a bottom-up statistical channel generator was presented in [22]. In this model, an abstract statistical description of a simple topology was made, followed by the application of the ABCD matrix approach to derive the CFR. This approach allowed also to model the channel periodic time variations by adding a number of time variant loads, as it was done in [30]. A more realistic statistical description of in-home networks was offered in [13]. Herein, a voltage-ratio approach was also proposed to efficiently obtain the channel transfer function in complex networks with many nested branches. The statistics of the in-home channel were inferred in [31] as a function of different network parameters, as wiring structures, size, and loads.

3.1 Random Vector Channel Model

In this section, we show that it is possible to use a new and conceptually simple approach to model the BB channel. To start, let us express the CFR in amplitude and phase, as $H(f) = r(f)e^{i\varphi(f)}$. Then, if we knew the joint statistics of the amplitude $r(f)$ and the phase $\varphi(f)$ we could generate the CFR. The characterization of the channel from measurements has shown that the amplitude is well fitted by the log-normal distribution, while the phase has a uniform distribution. However, both of them exhibit a correlation among different frequencies. To proceed, we consider the logarithm of the CFR, defined as follows

$$H_{dB}(f) = \log\left[r(f)\right] + i\varphi(f) = \gamma(f) + i\varphi(f). \tag{7}$$

where $\gamma(f)$ is the CFR amplitude in dB with mean $m(f)$ while $\varphi(f)$ is the phase with zero mean. The covariance of the CFR in dB is given by

$$\begin{aligned} R(f,\nu) &= E\left[(H_{dB}(f) - m_{H_{dB}}(f))(H_{dB}(\nu) - m_{H_{dB}}(\nu))^*\right] \\ &= R^{\gamma}(f,\nu) + R^{\varphi}(f,\nu) + i[R^{\gamma,\varphi}(\nu,f) - R^{\gamma,\varphi}(f,\nu)], \end{aligned} \tag{8}$$

where f and ν identify the frequencies, while $R^{\gamma}(\cdot)$, $R^{\varphi}(\cdot)$ and $R^{\gamma,\varphi}(\cdot)$ are the auto-covariance of the real part, the imaginary part and the covariance among the real and the imaginary part, respectively. Potentially, the knowledge of the covariance can lead us to model the channel in a certain frequency band, i.e., in a certain discrete number of frequencies, as a vector of correlated random variables with a certain covariance matrix. This is what will be done in the following considering the in-home channel in the 1.8–100 MHz frequency band. As a term of comparison of the correlation among the variables we refer to the normalized covariance matrix as the covariance matrix normalized by the product of the standard deviations of the considered variables. As the correlation, the normalized covariance matrix changes from 0 to 1.

3.1.1 In-Home Random Vector Channel Model

According to previous works [14], [32], [33], it is known that the amplitude (in dB) $\gamma(f)$ for the in-home scenario is well modeled by a normal distribution with a certain mean. The phase $\varphi(f)$ is uniformly distributed in the interval $(-\pi, \pi)$ [33]. From our database of 1300 responses we have computed the normalized covariance matrix among $\gamma(f)$ and $\varphi(f)$ in the frequency range 1.8–100 MHz, showing an average correlation coefficient $\bar{\rho}^{\gamma,\varphi} = 0.033$ (with a maximum value of $\rho_{\max}^{\gamma,\varphi} = 0.158$). Since $\bar{\rho}^{\gamma,\varphi} = E_{f,\nu}[R^{\gamma,\varphi}(f,\nu)] \cong 0$, we can assume that $\gamma(f)$ and $\varphi(f)$ are uncorrelated. Although, uncorrelation does not imply statistical independence, to provide a simple description of the model, in the following we assume them to be independent. Moreover, the normalized covariance matrix of the experimental channels in dB scale has been computed. Analyzing the imaginary part, it can be noted that the average value $\bar{\rho}^{H_{dB},img} = 0.024$ (with a maximum value of $\rho_{\max}^{H_{dB},img} = 0.130$) is quite low. Thus, according to equation (8), we can assume $R^{\gamma,\varphi}(\nu,f) - R^{\gamma,\varphi}(f,\nu) \cong 0$. Hence, the covariance of the experimental measures in dB scale is real and is equal to the sum of the covariance of the amplitude and the phase (8). Therefore, in the rest of this section, we discuss results concerning only the real part of the covariance matrix of H_{dB}.

In summary, the CFR (in dB) generation simplifies into the generation of a vector of correlated normal variables plus a vector of correlated uniform random variables. In order to generate correlated amplitudes, the normality of $\gamma(f)$ can be exploited, as done in [32], so that $\hat{\gamma}_{dB}^{cor} = (\mathbf{K}^{\gamma})^{1/2}\hat{\gamma}_{dB}^{ind} + \mathbf{m}$, where $\mathbf{K}^{\gamma}$ is the $N \times N$ amplitude covariance matrix, while $\hat{\gamma}_{dB}^{ind}$ is the vector of independent normal variables of size N, that is equal to the considered number of frequency samples. Furthermore, $\mathbf{m} = E[\mathbf{H}_{dB}]$ is the average amplitude obtained from the experimental measures.

Instead, the generation of a vector of uniform random variables with normalized covariance matrix $\mathbf{\Sigma}$ requires a more complex procedure described in the following steps. The procedure can be derived by recalling the relation existing between the Pearson (linear) and the Spearman (rank) correlation for normal variables, some details of which are reported in the Appendix [34]. Thus, let $\mathbf{\Sigma}$ be the target normalized covariance matrix. Let $F(\cdot)$ be the normal distribution function. Then, we generate a vector of normal r.v. with normalized covariance matrix $\hat{\mathbf{\Sigma}} = 2\sin(\mathbf{\Sigma}\pi/6)$. Finally, we obtain the vector of correlated uniform r.v. as $\mathbf{u} = F(\mathbf{x})$.

The comparison among the normalized covariance matrices of the CFR in dB scale for the measured channels (on top) and the simulated channels (on bottom) is depicted in Fig. 5 in absolute value. The range of possible values from 0 to 1 are represented by a monochromatic scale from clear to dark, respectively. As can be noted, the normalized covariance is particularly high among neighboring frequencies (around the main diagonal). However, even for very far away frequencies, the values are still pronounced (in the order of 0.3–0.4). The comparison shows that the difference among the experimental and the simulated channels normalized covariance matrix is very small and only few regions (especially those close to the transition between high (~0.9) and low (~0.3) covariance) show a slight difference. This is most likely due to numerical approximations and the assumed approximated statistics of the amplitude and phase.

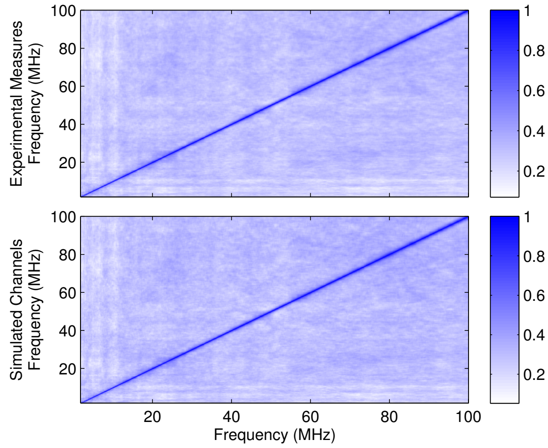

Fig. 5 Normalized covariance matrix of the logarithm version of the experimental measures (on top) and of the simulated channel realizations (on bottom) in the 1.8–100 MHz frequency band.

4. Inferring the Physical Layer Performance

From the channel and noise characterization, we can infer the performance achievable at the physical layer by computing the channel capacity. This is herein done under the assumption of Gaussian background noise. It has to be emphasized that the true capacity of the PLC channel is still unknown since the statistics of the noise has not been thoroughly investigated yet. More in detail, we consider the in-home case and we infer the improvement provided by the frequency band extension from 1.8–30 to 1.8–100 MHz. Moreover, concerning the range 1.8–30 MHz, we consider both the outdoor LV and MV scenarios. Furthermore, beside the theoretical capacity, also the achievable rate obtained through the use of CB-FMT and OFDM transmitting schemes has been evaluated for all the scenarios, as it will be discussed in the next section. Fig. 6 depicts the achievable rate complementary CDF (C-CDF) for the theoretical case for the indoor and outdoor LV and MV environments. We assume a −50 dBm/Hz transmitted PSD constraint in the 1.8–30 MHz and a flat −80 dBm/Hz PSD in the 30–100 MHz. Notching is typically required in BB PLC to allow coexistence with radio amateur and broadcast signals. Therefore, the PSD notching mask depicted in Fig. 7 is herein used to derive results. The colored background noise models, named in-home (best), outdoor LV and outdoor MV in Section 2.4, are herein adopted for each different environment, respectively. Fig. 6a, beside the C-CDF of the experimental measures, also reports the curves obtained using the vector channel model presented in Section 3.1.1. Furthermore, it shows that there is a good agreement between the C-CDF obtained with the experimental channels and with the simulated ones. Moreover, the extension of the frequency band provides a significant performance improvement. However, this improvement is not proportional to the bandwidth enlargement. In this respect, we can define the spectral efficiency η as the ratio between the maximum achievable rate and the transmission bandwidth. The spectral efficiency coefficient for the in-home 1.8–30 MHz case is $\eta_1 = 13.42$, while for the 1.8–100 MHz is $\eta_2 = 7.54$, with similar values for both experimental and simulated chan-

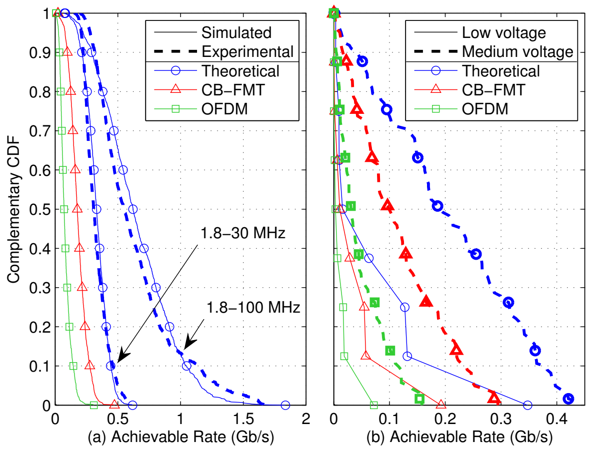

Fig. 6 Achievable rate C-CDF for in-home (on left) and outdoor LV and MV (on right): theoretical case, CB-FMT and OFDM.

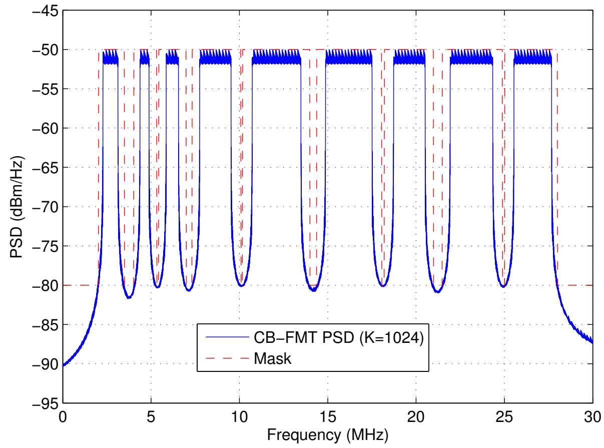

Fig. 7 CB-FMT PSD for $K = 1024$ and the target HP notching mask.

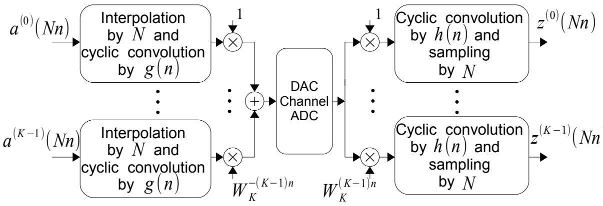

Fig. 8 CB-FMT baseline transceiver scheme.

nels. As can be noted, η decreases as the bandwidth increases. This is due to a lower transmission PSD limit in the band beyond 30 MHz (−80 rather than −50 dBm/Hz, as required by the HPAV2 [2]) and to a larger channel attenuation (PLC networks have a typical frequency decreasing path loss profile). This, results in a small SNR and thus in a reduced rate gain per bandwidth extension.

As can be seen in Fig. 6b, the MV outperforms the LV scenario in terms of achievable rate C-CDF. Although the MV noise PSD is higher than that of the LV scenario (see Fig. 4), the MV environment is affected by a lower channel attenuation, as depicted in Fig. 3.

5. Filter Bank Modulation

Both NB and BB state-of-the-art PLC systems deploy multicarrier modulation (MCM) at the physical layer. In MCM a high data rate information sequence is split in a series of K low data rate sequences transmitted in one of the sub-bands in which the wide band spectrum has been partitioned. The k-th data signal, $a^{(k)}(\ell N)$, comprises a stream of complex data symbols belonging to a certain constellation, e.g., M-QAM or M-PSK, transmitted with normalized period N. The MCM transmitter can be viewed as a synthesis filter bank (FB) where the low-data rate information sequences are interpolated by a factor N and, then, filtered with a prototype pulse that is identical for all sub-channels. The filter outputs are multiplied by a complex exponential to obtain a spectrum translation. Finally, the K modulated signals are summed together yielding the discrete time signal

$$x(n) = \sum_{k=0}^{K-1} \sum_{\ell \in Z} a^{(k)}(\ell N) g(n - \ell N) W_K^{-nk}, \quad n \in Z, \tag{9}$$

where $g(n)$ is the prototype pulse and $W_K^{-nk} = e^{j2\pi nk/K}$ is the complex exponential function. The receiver can be seen as an analysis FB where the received signal $y(n) = x * h_{CH}(n) + \eta(n)$, with $*$, $h_{CH}(n)$, and $\eta(n)$ denoting the linear convolution operator, the discrete time channel impulse response and the additive background noise, is multiplied by a bank of complex exponential functions. The obtained signals are filtered with a prototype pulse $h(n)$ and, finally, sampled by a factor N. The n-th sample in the k-th sub-channel output is then given by

$$z^{(k)}(nN) = \sum_{\ell \in Z} y(\ell) W_K^{\ell k} h(nN - \ell). \tag{10}$$

Specific schemes can be realized depending on the choice of the FB design, e.g., OFDM, FMT, OQAM/OFDM [1]. If the prototype pulse $g(n)$ is a rectangular time window the popular OFDM [35] solution will be obtained. If a more relaxed window is used, e.g., a raised cosine window in time, pulse shaped OFDM will be obtained. For instance, ITU G.hnem, HPAV, IEEE P1901 and ITU G.hn use all pulse shaped OFDM. If on the contrary, the sub-channel frequency confinement is privileged, then the filtered multitone (FMT) modulation solution will be obtained [36], [37]. In such a case, a possible choice consists in the use of a truncated root-raised-cosine prototype pulse. An orthogonal FB design is also possible as described in [38]. The rationale for the deployment of FB modulation in PLC is due to the fact that the channel is severely frequency selective. Consequently, the equalization task in single carrier modulation can be too complex. On the contrary, for instance, in FMT the sub-channels are well frequency confined, therefore the inter-channel interference (ICI) is negligible while the residual sub-channel inter-symbol interference (ISI) can be mitigated with simple one-tap sub-channel equalization. Furthermore, FB modulation allows to op-

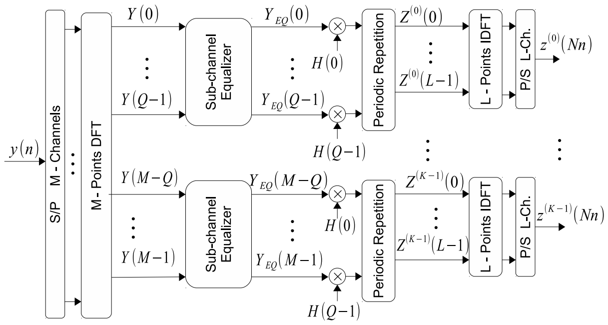

Fig. 9 Frequency domain implementation of the CB-FMT receiver, with $Q = M/K$ frequency samples per sub-channel.

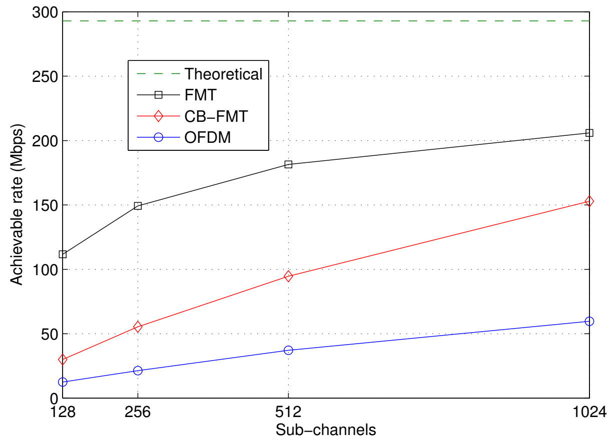

Fig. 10 Comparison between FMT, CB-FMT and OFDM as a function of the sub-channel number K in terms of maximum achievable rate.

timally allocate resources through bit and power loading across the sub-channels, thus approaching capacity. In PLC, it is also important to offer spectrum agility by implementing notching of parts of the spectrum. This is because coexistence with radio systems operating in the same spectrum must be granted. Although this can be done with conventional OFDM, its poor sub-channel frequency confinement offers poor notching selectivity. In detail, to respect a certain notching mask, an excessive number of sub-channels must be switched off so that a significant data rate penalty is introduced. This justifies the proposal to use FB modulation where the FB is designed to have good sub-channel frequency localization properties. In addition, to grant high flexibility, the FB parameters can be adapted to the channel conditions. For instance, in OFDM the cyclic prefix (CP) length can be adjusted to offer the highest capacity [39]. Similarly, this can be done in FMT by adapting the pulse shape and the interpolation factor N [1].

As an example, in Fig. 10 we report the achievable rate in Mbps as a function of the number of sub-channels K used for OFDM for a specific channel realization (corresponding to the median channel ranked in terms of capacity selected from the database of measured channels). The CP length is chosen so that the highest rate is offered under the further constraint of fulfilling the notching mask in Fig. 7. The noise PSD is the best according to the model in Fig. 4. The figure shows that the offered rate increases with the number of sub-channels since the overhead introduced by the CP is reduced and better notching capability is obtained. However, the performance gap from the channel capacity is high. Such a gap can be reduced by deploying FMT. In this example, FMT uses long root-raised-cosine pulses with roll-off set to 0.2 and one-tap sub-channel fractionally spaced equalization. The interpolation factor is equal to $N = 4/3K$ and the filter length is equal to $20N$. Therefore, significantly better notching capability is achieved.

However, the use of long prototype pulses increases the implementation complexity. The efficient polyphase discrete Fourier transform (DFT) based realization has a complexity that grows with the pulse length [38]. It is therefore important to design short prototype pulses with good time/frequency localization.

In order to reduce the complexity in FMT, recently, the use of a different architecture where the linear convolutions in (9) are replaced with circular convolutions has been proposed [40]. Furthermore, the transmission takes place in blocks, similarly to OFDM. The scheme is referred to as cyclic block FMT (CB-FMT). The CB-FMT scheme is sketched in Fig. 8. The CB-FMT transmitted signal can be written, for $n \in \{0, \cdots, M-1\}$, as

$$x(n) = \sum_{k=0}^{K-1} \sum_{\ell=0}^{L-1} a^{(k)}(\ell N) g((n-\ell N)_M) W_K^{-nk}, \tag{11}$$

where $g((n)_M)$ denotes the periodic repetition of the prototype pulse $g(n)$ with a period equal to M, i.e., $g((n)_M) = g(mod(n, M))$ where $mod(\cdot, \cdot)$ is the modulo operator.

The circular convolution is applied also in the analysis FB at the receiver. This allows to realize an efficient frequency domain implementation [41]. In Fig. 9, the CB-FMT receiver efficient implementation is shown. It comprises: a DFT of $M = LN$ points equal to the prototype pulse length, a sub-channel equalizer, matching the output signals with the filter coefficients $H(i) = G^*(i)$ where $G(i)$ denotes the DFT of the prototype pulse, a periodic repetition, and a final IDFT of L points. The sub-channel equalizer can be designed according to the MMSE criterion [42].

Now, in Fig. 10 the achievable rate for CB-FMT is shown. For CB-FMT, a rectangular frequency domain pulse is used (which renders the system to be the dual of OFDM). The interpolation factor is equal to $N = K$ and the filter length is equal to $4K$. For both CB-FMT and OFDM a CP is added to the transmitted signal to reduce the interference between different blocks. The CP duration is optimized to maximize the achievable rate. Fig. 10 shows that CB-FMT provides better performance than OFDM. For $K = 1024$, CB-FMT is not far away from FMT but it has significant less complexity, i.e. the CB-FMT complexity is about 36% of the FMT complexity. The ability of providing good notching selectivity is shown in Fig. 7, where the PSD of the transmitted CB-FMT signal is compared to the target notching mask. Going back to Fig. 6, CB-FMT outperforms OFDM in the 1.8–30 MHz band in terms of achievable rate, offering about 51%, 45% and 51% of the theoretical channel capacity, for the in home, LV and MV channels, respectively.

6. Conclusions

PLC has become a mature technology that can find application in many different scenarios: from in-home automation and networking, to smart grid applications, to in-vehicle communications. Despite the existence of recently standardized NB and BB PLC systems, there exists space for their further evolution. A challenging aspect is the design of reliable communication techniques that can cope with the nasty channel. We have described the main characteristics of the PLC channel for different scenarios showing that in all cases severe frequency selectivity and attenuation is exhibited. Nevertheless, the inferred capacity (under the Gaussian noise assumption) is high and motivates the development of capacity approaching schemes. Among them, filter bank modulation has the ability to offer high spectral efficiency, spectrum agility and adaptive notching for coexistence with radio systems operating in the same band. Among the filter bank modulation schemes, FMT has the potentiality of providing higher performance than OFDM given its better sub-channel spectral containment and the ability to better exploit the channel diversity through sub-channel equalization. However, its complexity can be higher. Therefore, simple realizations are advisable. In this respect, we have presented cyclic block FMT which follows the idea of synthesizing well frequency localized sub-channels. However, the filter bank uses circular convolutions instead of linear ones. CB-FMT has lower complexity than FMT and still has the potentiality of improving the OFDM performance.

References

[1] H.C. Ferreira, L. Lampe, J. Newbury, and T.G. Swart, Power Line Communications: Theory and Applications for Narrowband and Broadband Communications over Power Lines, Wiley & Sons, NY, 2010.

[2] L. Yonge, K. Afkhamie, L. Guerrieri, S. Katar, H. Lioe, P. Pagani, R. Riva, D.M. Schneider, and A. Schwager, "An Overview of the HomePlug AV2 Technology," Journal of Electrical and Computer Engineering, vol.2013, pp.1–20, 2013.

[3] "IEEE Standard for Broadband over Power Line Networks: Medium Access Control and Physical Layer Specifications." IEEE 1901-2010, Sept. 2010.

[4] "Unified High-Speed Wireline-Based Home Networking Transceivers - System Architecture and Physical Layer Specification." Recommendation ITU-T G.9960, Dec 2011.

[5] IEC, Distribution automation using distribution line carrier systems - Part 5-1: Lower layer profiles - The spread frequency shift keying (S-FSK) profile (IEC 61334-5-1, ed. 2.0), May 2001.

[6] "Narrowband Orthogonal Frequency Division Multiplexing Power Line Communication Transceivers for PRIME Networks." Recommendation ITU-T G.9904, 2012.

[7] "Narrowband Orthogonal Frequency Division Multiplexing Power Line Communication Transceivers for G3-PLC Networks." Recommendation ITU-T G.9903, 2012.

[8] "Narrowband Orthogonal Frequency Division Multiplexing Power Line Communication Transceivers for ITU-T G.hnem networks." Recommendation ITU-T G.9902: Narrowband, Oct. 2012.

[9] "IEEE Standard for Low-Frequency (less than 500 kHz) Narrowband Power Line Communications for Smart Grid Applications." IEEE 1901.2-2013, Dec. 2013.

[10] S. Goel, S.F. Bush, and D. Bakken, eds., IEEE Vision for Smart Grid Communications: 2030 and Beyond, IEEE Std. Association, 2013.

[11] F. Corripio, J. Arrabal, L. del Rio, and J. Munoz, "Analysis of the cyclic short-term variation of indoor power line channels," IEEE J. on Selected Areas in Commun., vol.24, no.7, pp.1327–1338, 2006.

[12] M. Antoniali and A.M. Tonello, "Measurement and characterization of load impedances in home power line grids," IEEE Trans. on Instrumentation and Measurements (in press), 2013.

[13] A.M. Tonello and F. Versolatto, "Bottom-Up Statistical PLC Channel Modeling - Part I: Random Topology Model and Efficient Transfer Function Computation," IEEE Trans. Power Del., vol.26, no.2, pp.891–898, April 2011.

[14] S. Galli, "A Novel Approach to the Statistical Modeling of Wireline Channels," IEEE Trans. Commun., vol.59, no.5, pp.1332–1345, May 2011.

[15] J.A. Cortés, F.J. Cañete, L. Díez, and J.L.G. Moreno, "On the Statistical Properties of Indoor Power Line Channels: Measurements and Models," Proc. Int. Symp. on Power Line Commun. and Its App. (ISPLC), pp.271–276, April 2011.

[16] M. Tlich, A. Zeddam, A. Moulin, and F. Gauthier, "Indoor Power-Line Communications Channel Characterization up to 100 MHz - Part II: Time-Frequency Analysis," IEEE Transactions on Power Delivery, vol.23, no.3, pp.1402–1409, July 2008.

[17] M. Antoniali, A.M. Tonello, M. Lenardon, and A. Qualizza, "Measurement and Analysis of PLC Channels in a Cruise Ship," Proc. of Int. Symp. on Power Line Commun. and Its App. (ISPLC), pp.102–107, April 2011.

[18] M. Mohammadi, L. Lampe, S.M. M. Lok, M. Mirvakili, R. Rosales, and P. van Veen, "Measurement Study and Transmission for In-Vehicle Power Line Communication," Proc. of Int. Symp. on Power Line Commun. and Its App. (ISPLC'09), pp.73–78, 2009.

[19] M. Antoniali, M. De Piante, and A.M. Tonello, "PLC Noise and Channel Characterization in a Compact Electrical Car," Proc. of IEEE Int. Symp. on Power Line Commun. and Its App. (ISPLC), pp.29–34, March 2013.

[20] M. Babic *et al.*, "D4: "Theoretical Postulation of the PLC Channel Model OPERA"," tech. rep., IST Integrated Project No. 507667 funded by EC, March 2005. OPERA Deliverable D4.

[21] A.M. Tonello, F. Versolatto, and C. Tornelli, "Analysis of Impulsive UWB Modulation on a Real MV Test Network," Proc. of IEEE Int. Symp. on Power Line Commun. and Its App. (ISPLC), pp.18–23, 3–6 April 2011.

[22] T. Esmailian, F.R. Kschischang, and P. Glenn Gulak, "In-Building Power Lines as High-Speed Communication Channels: Channel Characterization and a Test Channel Ensemble," Intern. J. of Commun. Syst., vol.16, no.5, pp.381–400, June 2003.

[23] M. Babic *et al.*, "D5 Pathloss as a function of frequency, distance and network topology for various LV and MV European powerline networks.," tech. rep., IST Integrated Project No. 507667, April 2005. OPERA Deliverable D5.

[24] A. Tonello, F. Versolatto, and M. Girotto, "Multitechnology (I-UWB and OFDM) Coexistent Communications on the Power Delivery Network," IEEE Trans. Power Del., vol.28, no.4, pp.2039–2047, 2013.

[25] M. Zimmermann and K. Dostert, "A Multipath Model for the Powerline Channel," IEEE Trans. Commun., vol.50, no.4, pp.553–559, April 2002.

[26] A.M. Tonello, "Wideband Impulse Modulation and Receiver Algorithms for Multiuser Power Line Communications," EURASIP Journal on Advances in Signal Processing, vol.2007, pp.1–14, 2007.

[27] A.M. Tonello, F. Versolatto, B. Béjar, and S. Zazo, "A Fitting Algorithm for Random Modeling the PLC Channel," IEEE Trans. Power

Del., vol.27, no.3, pp.1477–1484, June 2012.
[28] M. Tlich, A. Zeddam, A. Moulin, and F. Gauthier, "Indoor Power-Line Communications Channel Characterization Up to 100 MHz - Part I: One-Parameter Deterministic Model," IEEE Transactions on Power Delivery, vol.23, no.3, pp.1392–1401, July 2008.
[29] H. Meng, Y.L. Guan, C.L. Law, P.L. So, E. Gunawan, and T. Lie, "Modeling of Transfer Characteristics for the Broadband Power Line Communication Channel," IEEE Trans. Power Del., vol.19, no.3, pp.1057–1064, July 2004.
[30] F. Canete, J. Cortes, L. Diez, and J. Entrambasaguas, "A channel model proposal for indoor power line communications," Communications Magazine, IEEE, vol.49, no.12, pp.166–174, 2011.
[31] A. Tonello and F. Versolatto, "Bottom-Up Statistical PLC Channel Modeling—-Part II: Inferring the Statistics," IEEE Transactions on Power Delivery, vol.25, no.4, pp.2356–2363, 2010.
[32] A. Pittolo and A.M. Tonello, "Physical Layer Security in PLC Networks: An Emerging Scenario, Other Than Wireless," IET Commun., Special Issue: Secure Physical Layer Commun., July 2013.
[33] F. Versolatto and A.M. Tonello, "PLC Channel Characterization up to 300 MHz: Frequency Response and Line Impedance," Proc. IEEE Global Commun. Conf. (GLOBECOM), pp.3525–3530, Dec 2012.
[34] M. Gili, D. Maringer, and E. Schumann, Numerical Methods and Optimization in Finance, ch. 7: Modeling dependencies, pp.165–173, Access Online via Elsevier, 2011.
[35] J. Bingham, "Multicarrier Modulation for Data Transmission, an Idea whose Time Has Come," IEEE Commun. Mag., vol.31, pp.5 – 14, May 1990.
[36] G. Cherubini, E. Eleftheriou, and S. Olcer, "Filtered Multitone Modulation for Very High-Speed Digital Subscribe Lines," IEEE J. Sel. Areas Commun., pp.1016–1028, June 2002.
[37] A. Tonello and F. Pecile, "Efficient Architectures for Multiuser FMT Systems and Application to Power Line Communications," IEEE Trans. Commun., vol.57, no.5, pp.1275–1279, 2009.
[38] N. Moret and A.M. Tonello, "Design of Orthogonal Filtered Multitone Modulation Systems and Comparison among Efficient Realizations," EURASIP Journal on Advanced Signal Processing, 2010.
[39] A. Tonello, S. D'Alessandro, and L. Lampe, "Cyclic Prefix Design and Allocation in Bit-Loaded OFDM over Power Line Communication Channels," IEEE Trans. Commun., vol.58, no.11, pp.3265–3276, 2010.
[40] A.M. Tonello and M. Girotto, "Cyclic Block FMT Modulation for Broadband Power Line Communications," Proc. of IEEE Int. Symp. on Power Line Commun. and Its App. (ISPLC 2013), Johannesburg, South Africa, pp.247–251, March 2013.
[41] A.M. Tonello, "A Novel Multi-carrier Scheme: Cyclic Block Filtered Multitone Modulation," Proc. of IEEE Int. Conf. on Commun. (ICC 2013), Budapest, Hungary, pp.3856–3860, June 2013.
[42] A.M. Tonello and M. Girotto, "Cyclic Block Filtered Multitone Modulation," EURASIP J. on Advanced Sig. Proc., submitted to.

7. Appendix

Herein, we briefly discuss the procedure to generate uniformly distributed random variables $\mathbf{u} \sim \mathcal{U}(0, 1)$ that exhibit a certain correlation matrix $\mathbf{\Sigma}$, [34]. Given a distribution function $F(\cdot)$, it is well known that a multivariate random variable (r.v.) $\mathbf{x} = F^{-1}(\mathbf{u})$ has distribution $F(\cdot)$. By reversing this expression, uniformly distributed variables can be generated starting, for instance, from a Gaussian distribute r.v.. Generate a vector of correlated Gaussian r.v. is simple. However, the Pearson (or linear) correlation is not necessarily invariant to transformations. Nevertheless, the Spearman correlation (also called rank or fractile correlation), is invariant to any strictly increasing transformation, such as $F(\cdot)$, which is monotonically increasing in our case. In particular, given two distributions, $F(\cdot)$ and $G(\cdot)$, and two multivariate r.v. $\mathbf{x} \sim F$ and $\mathbf{y} \sim G$, Spearman and Pearson correlation are related according to the equation $\rho^S_{\mathbf{x},\mathbf{y}} = \rho^P_{F(\mathbf{x}),G(\mathbf{y})}$, where S stands for Spearman and P for Pearson. For the normal distribution, the exact relationship between Spearman and Pearson correlation is known and it is equal to $\rho^P = 2\sin\left(\frac{\pi}{6}\rho^S\right)$ [34]. It follows that the generation of a vector of uniform r.v. with correlation $\mathbf{\Sigma}$ can be obtained by a vector of normal r.v. with covariance matrix $\hat{\mathbf{\Sigma}}$.

Andrea M. Tonello is an Aggregate Professor at the University of Udine, Italy (since 2003) where he leads the Wireless and Power Line Communication Lab. He is also the founder of WiTiKee, a university spin-off company working in the field of telecommunications for the smart grid. From 1997 to 2002 he has been with Bell Labs Lucent Technologies firstly as a Member of Technical Staff and then as a Technical Manager at the Advanced Wireless Technology Laboratory, Whippany, NJ and the Managing Director of the Bell Labs Italy division. He obtained the Laurea degree (1996) and the Doctor of Research degree in electronics and telecommunications (2003) from the University of Padova, Italy. Dr. Tonello received the Full Professor Habilitation in 2013 and several recognitions among which the Lucent Bell Labs Recognition of Excellence (1999), the Distinguished Visiting Fellowship from the Royal Academy of Engineering, UK (2010) and the Distinguished Lecturer Award by the IEEE Vehicular Technology Society (2011-15). He also received (as co-author) five best paper awards. He is the Chair of the IEEE Communications Society Technical Committee on Power Line Communications. He serves/ed as an Associate Editor for the IEEE Transactions on Vehicular Technology (2007-2013), for the IEEE Transactions on Communications (since 2012) and IEEE Access (since 2013). He served as the general chair of IEEE ISPLC 2011 and he is the general co-chair of IEEE SmartGridComm 2014.

Alberto Pittolo received from the University of Udine, Udine, Italy, the Laurea degree in electrical engineering (2009) and the Laurea Specialistica degree (2012) in electrical and telecommunications engineering, with honors. He is currently pursuing the Ph.D. His research interests and activities are channel modeling, resource allocation and physical layer security for both wireless and power line communications.

Mauro Girotto (GSM'12) received the Laurea degree (2008) and the Laurea Specialistica degree (2012) in electrical engineering with honors from the University of Udine, Udine, Italy, where he is currently pursuing the Ph.D. His research interests are filter bank modulation schemes for wireless and power line communications.